

# Pseudospectral versus finite difference schemes for the Kardar-Parisi-Zhang equation with long-range temporally correlated noise

Xiongpeng Hu and Hui Xia\*

*School of Materials Science and Physics, China University of Mining and Technology, Xuzhou 221116, China*

(Dated: November 8, 2021)

To investigate universal behavior and effects of long-range temporal correlation in kinetic roughening, we perform extensive simulations of the Kardar-Parisi-Zhang (KPZ) with temporally correlated noise based on pseudospectral (PS) and one of the improved finite difference (FD) schemes. We find that scaling properties are obviously affected by long-range temporal correlations within the effective temporal correlated regions. Our results are consistent with each other using these two independent numerical schemes. The difference between these two characteristic roughness exponents  $\alpha_s$  and  $\alpha$  becomes larger as  $\theta$  increases, and the local roughness exponent  $\alpha_{loc}$  exhibits non-universal scaling within local window sizes. Our results also show that PS and the improved FD schemes could be effective to suppress numerical instabilities in the temporal correlated KPZ growth equation. Furthermore, our investigations imply that, when the effects of long-range temporal correlation are not ignored, the continuum and discrete growth systems do not belong to the same universality class, even with the same temporal correlated exponent.

PACS numbers: 05.40.-a, 45.10.Hj, 02.60.Cb

Keywords: kinetic roughening; Kardar-Parisi-Zhang growth; Pseudospectral approach; long-range temporal correlation

## I. INTRODUCTION

In recent years, an enormous amount of work has been devoted to studying kinetic roughening, which has attracted much attention due to its many critical applications as molecular beam epitaxy, bacterial growth, fluid flow in porous media, etc[1]. A few discrete models, such as the Eden, ballistic deposition (BD) and restricted solid-on-solid (RSOS) models, were proposed to describe various interface growth[2, 3]. Fortunately, the large-scale dynamics of such growth systems may be essentially described in terms of continuum stochastic partial differential equations of the Langevin-type form, which is also a continuous approximation of the discrete model. One of the most well-known Langevin-type growth systems is the Kardar-Parisi-Zhang (KPZ) equation[4], representing one important universality class of surface growth, reads

$$\partial_t h(\mathbf{x}, t) = \nu \nabla^2 h + \lambda (\nabla h)^2 + \eta(\mathbf{x}, t), \quad (1)$$

where  $h(\mathbf{x}, t)$  is the height on a  $d$ -dimensional substrate at position  $\mathbf{x}$  and time  $t$ ,  $\nu$  is effective surface tension,  $\lambda$  characterizes the tilt-dependence of the growth velocity, and  $\eta(\mathbf{x}, t)$  is Gaussian noise with  $\langle \eta(\mathbf{x}, t) \eta(\mathbf{x}', t') \rangle = 2D\delta^d(\mathbf{x} - \mathbf{x}')\delta(t - t')$ .

In order to conveniently perform numerical integration, Eq. (1) can be transformed by rescaling of the parameters into the reduced equation with only one independent control parameter, namely coupling constant  $g = \lambda \sqrt{2D/\nu^3}$ , which means that we can set  $\nu$  and  $D$  to 1 and then replace  $\lambda$  with  $g$ . For a system of size  $L$ , the interface width  $W(L, t)$  can be expressed in the dynamic scaling form[5]

$$W(L, t) \equiv \left\langle \frac{1}{L} \sum_{i=1}^L [h(\mathbf{x}_i, t) - \bar{h}(t)]^2 \right\rangle^{1/2} \sim L^\alpha f\left(\frac{t}{L^z}\right), \quad (2)$$

where  $\langle \dots \rangle$  represents ensemble average,  $\alpha$  and  $z$  are the roughness and dynamic exponents, respectively. The universal scaling function  $f(u)$  has specific asymptotic properties such that  $W(L, t) \sim t^\beta$  for  $t \ll L^z$  and  $W(L, t) \sim L^\alpha$  for  $t \gg L^z$ . The ratio  $\beta = \alpha/z$  is the growth exponent characterizing the time-dependent dynamics of the roughening process. The KPZ equation with uncorrelated noise has scale-invariant solutions, as proven by dynamic renormalization group (DRG) technique[4]. For  $(1+1)$ -dimensions,  $\alpha = 1/2$ ,  $\beta = 1/3$ , and  $z = 3/2$ . Furthermore, the KPZ equation satisfies Galilean invariance in any dimension, which implies there exists the hyper-scaling relation  $\alpha + z = 2$ . In contrast, exact exponents are not known due to the existence of a strong-coupling fixed point for  $d > 1$ .

Since the exact solution of the KPZ equation is hardly obtained due to its inherent nonlinear characteristics, the situation is even more complicated when the correlated noise is present. Furthermore, spatially or temporally correlated noise modifies the universality class, allowing the continuous tuning of the scaling exponents within certain limits[1]. The long-range spatiotemporally correlated noise has the form

$$\langle \eta(\mathbf{x}, t) \eta(\mathbf{x}', t') \rangle = |\mathbf{x} - \mathbf{x}'|^{2\rho-d} |t - t'|^{2\theta-1}, \quad (3)$$

where  $\rho$  and  $\theta$  are two exponents characterizing the decay of spatial and temporal correlations, respectively. Using DRG calculations, Medina et al.[6] found that, for sufficiently small  $\rho$  and  $\theta$ , the critical exponents are the same

\* [hxia@cumt.edu.cn](mailto:hxia@cumt.edu.cn)

as those for uncorrelated noise. For  $\rho$  or  $\theta$  beyond certain critical values, the correlations become relevant, and then the scaling exponents are nontrivial functions of  $\rho$  and  $\theta$ .

While the effect of spatially correlated noise ( $\rho \neq 0, \theta = 0$ ) in the KPZ system has been extensively studied in the literatures [7–26], only a few investigations carried out in the KPZ equation with long-range temporal correlations ( $\rho = 0, \theta \neq 0$ ) [27–33]. For this case, DRG method shows that, when  $0.167 < \theta < 0.5$ , the temporal correlation is relevant, and the exponents can be fitted to

$$\alpha(\theta) = 1.69\theta + 0.22, \quad \beta(\theta) = \frac{(1+2\theta)\alpha(\theta)}{2\alpha(\theta)+1}. \quad (4)$$

Numerical study on the BD model with temporally correlated noise [28], as the same universality class with KPZ driven by the same correlated noise, shows that, the results for  $\alpha$  and  $\beta$  are in good agreement with Eq. (4). But at  $\theta_c \cong 0.16$ , the results deviate from the scaling relation. This deviation suggests that the source of discrepancy is not in the numerical solution of the RG equation but instead in some uncontrollable crossover effects in the simulations [28]. Since the success of DRG techniques has been limited by the difficulties of reaching the strong-coupling regime, numerical simulations are often used as the most direct and definite ways to determine the universality class. As a common numerical method, finite-difference (FD) scheme has been widely explored the continuum KPZ dynamics [27–29, 34, 35]. It should be noted that, using FD scheme, numerical divergence always happens in the discretized version of the KPZ equation. In order to suppress the annoying growth instability, one can control it through replacing the square gradient of nonlinear terms by an exponential decaying technique, as suggested by Dasgupta et al. [36]. However, the exponentially decaying function is equivalent to the nonlinear term including infinitely many higher-order nonlinearities, which may change universal behavior in comparison with the original continuum growth system [37, 38].

Since conventional FD schemes are hampered by these discretization effects mentioned above, this unwanted scaling feature can be avoided in spectral shcemes [39–44]. The functional form of the stochastic continuum growth equation is guaranteed to be maintained [41]. Thus, the absence of uncontrolled discretization effects also allows us to compute various correlation functions and obtain critical exponents in a rather precise and reliable way. However, spectral scheme is rather time-consuming. To speed up the computation, one could adopt a pseudospectral (PS) approach, which is commonly used to deal with the nonlinear stochastic growth systems [39–43]. The only approximation made in the calculation being the truncation to a finite rather than a infinite number of modes.

On the one hand, much of the work in the local KPZ equation has examined that PS scheme gives results closer to the continuum limit than FD schemes [39–41, 43]. However, an improved FD scheme was pro-

posed by Lam and Shin [45], henceforth referred to as LS scheme. Using this improved FD scheme, the discretization of nonlinear term can effectively inhibit divergence compared with the standard forward-backward difference, i.e, central difference scheme. On the other hand, there are obvious differences between numerical simulations and analytical approximation methods of the KPZ equation with long-range temporally correlated noise [6, 27–29, 46]. Overall, it is necessary to further study the effects of temporally correlated noise on scaling properties. In this paper, we discuss the stability and overall performance of these numerical schemes, and apply PS and LS numerical schemes to the KPZ equation with temporally correlated noise clarifying universal behavior and investigating the effects of long-range temporal correlation in kinetic roughening.

The remaining of the paper is organized as follows. In Section II, we introduce the method to generate long-range temporally correlated noise and describe the general features of PS and LS schemes. Section III shows these numerical schemes to integrate the temporal correlated KPZ equation. Then the characteristic quantities and scaling exponents are computed, and nontrivial scaling are discussed. Conclusions and perspectives are included in Section IV

## II. BASIC METHODS AND CONCEPTS

### A. Long-range temporal correlated noise

To study such temporal correlated growth systems, we need to generate a random sequence  $\{\eta_i\}$  with long-range power-law correlation of the form

$$C(l) \equiv \langle \eta_i \eta_{i+l} \rangle \sim l^{2\theta-1} \quad (l \rightarrow \infty). \quad (5)$$

For this purpose, we utilize the fast fractional Gaussian noise generator (FFGN) proposed by Mandelbrot et al. [47, 48] and adopted by Lam et al. [28] to simulate the BD model with long-range temporally correlated noise. Using the FFGN method, the noise sequence  $\{\eta_i\}$  is defined as

$$\eta_i = \sum_{n=1}^N W_n X_i(u_n), \quad (6)$$

where  $W_n$  are weight factors for different characteristic frequencies and  $X_i$  represent Markov-Gaussian processes.  $N$  is the number of components needed, which should be increased to obtain the desired power-law exponent  $\theta$  with higher precision at low frequencies. By defining  $u_n = aB^{-n}$ ,  $r_n = e^{-u_n}$ ,  $B = 2$ ,  $a = 6$  and  $\{\zeta_i\}$  to be an uncorrelated sequence of uniform distribution in the interval  $[0, 1]$ ,  $W_n$  and  $X_i(u_n)$  can be constructed by

$$\begin{aligned} W_n^2 &= \frac{12(1-r_n^2)}{\Gamma(2-2\theta)} \left( B^{\frac{1}{2}-\theta} - B^{\theta-\frac{1}{2}} \right) u_n^{1-2\theta}, \\ X_1(u_n) &= (1-r_n^2)^{-0.5} (\zeta_1 - 0.5) \quad i = 1, \\ X_i(u_n) &= r_n X_{i-1}(u_n) + (\zeta_i - 0.5) \quad i > 1. \end{aligned} \quad (7)$$

It should be noted that another popular technique for generating long-range correlated noise is the Fourier filtering method (FFM)[26, 49]. However, this method requires generating the complete temporal sequence of random number for each site, and one has to generate a longer sequence of noise to achieve the fitting of power-law correlation function  $C(l)$ , which means that the FFM is more memory and time consuming than FFGN.

## B. Finite-differences scheme

Using FD scheme, by defining the positions  $x_i = i\Delta x (i = 0, \dots, N-1)$  of the nodes, the spatial derivatives of the right-hand side of Eq. (1) are discretized. For overall brevity, we define  $h_i(t) = h(x_i, t)$ . Using a one-step Euler method to compute the temporal derivative, the time evolution of KPZ in (1+1)-dimensions reads[35]

$$h(x_i, t+\Delta t) = h_i(t) + \Delta t [\nabla^2 h_i(t) + g(\nabla h_i)^2(t) + \eta_i(t)], \quad (8)$$

where  $\Delta t$  is the time step and  $\{\eta(x_i, t)\}$  is long-range correlated in the time direction generated by FFGN. Using standard forward-backward differences, the nonlinear term of Eq. (8) are, up to second order of approximation, given by

$$(\nabla h)^2(x_i, t) = \frac{1}{4}(\Delta x)^{-2} [h_{i+1}(t) - h_{i-1}(t)]^2. \quad (9)$$

Based on LS numerical scheme[45], the nonlinear term is discretized as

$$\begin{aligned} (\nabla h)^2(x_i, t) &= \frac{1}{3}(\Delta x)^{-2} \{ [h_{i+1}(t) - h_i(t)]^2 \\ &\quad + [h_{i+1}(t) - h_i(t)][h_i(t) - h_{i-1}(t)] \\ &\quad + [h_i(t) - h_{i-1}(t)]^2 \}. \end{aligned} \quad (10)$$

In LS discretization, the effective parameter  $g$  agrees with its nominal value. Notably, it has been argued that this discretization can recover the results of the continuum growth models while discrepancies arise in the use of conventional discretization[45].

## C. Pseudospectral scheme

PS scheme is another numerical scheme we adopted in this work, in which the spatial gradients are computed using the fast Fourier transform (FFT). Assuming that

the height field  $h(\mathbf{x}, t)$  satisfies periodic boundary conditions in the interval  $[0, L]$ , it can be described by Fourier modes  $\hat{h}(\mathbf{q}, t)$

$$h(\mathbf{x}, t) = \frac{1}{L} \sum_{k=-\frac{N}{2}}^{\frac{N}{2}-1} \hat{h}(q_k, t) e^{iq_k x} = \mathcal{F}^{-1}[\hat{h}(\mathbf{q}, t)], \quad (11)$$

where  $q_k = \frac{2\pi}{L} k$  represents the wave number. Applying the FFT to the temporal correlated KPZ equation, we obtain a set of ordinary differential equations (ODEs)

$$\frac{d\hat{h}_k(t)}{dt} = \hat{\mathcal{L}}_k(t) + g\hat{\mathcal{N}}_k(t) + \hat{\eta}_k(t). \quad (12)$$

The temporal discretization for the above complex equations is performed by a one-step Euler method. It is easy to verify that the Fourier modes  $\hat{\eta}_k(t)$  is derived from the Fourier transform of  $\eta(\mathbf{x}, t)$  with the correlations

$$\langle \hat{\eta}_k(t) \hat{\eta}_{k'}(t') \rangle \sim \delta_{k, -k'} |t - t'|^{2\theta-1}. \quad (13)$$

The calculation steps of the partial derivative are as follows

$$\begin{aligned} h(\mathbf{x}, t) &\rightarrow \text{FFT} \rightarrow \hat{h}(\mathbf{q}, t) \rightarrow (i\mathbf{q})^m \hat{h}(\mathbf{q}, t), \\ (i\mathbf{q})^m \hat{h}(\mathbf{q}, t) &\rightarrow \text{FFT}^{-1} \rightarrow \nabla^m h(\mathbf{x}, t). \end{aligned} \quad (14)$$

Thus, the linear term  $\hat{\mathcal{L}}_k(t)$  is given by

$$\hat{\mathcal{L}}_k(t) = -q_k^2 \hat{h}_k(t). \quad (15)$$

Using PS approach, alias appears when dealing with nonlinear terms, and the wave number in convolution exceeds the range of frequency. The nonlinear term  $\hat{\mathcal{N}}_k(t)$  leads to a convolution

$$\begin{aligned} \hat{\mathcal{N}}_k(t) &= - \sum_{k_1+k_2=k} q_{k_1} q_{k_2} \hat{h}_{k_1}(t) \hat{h}_{k_2}(t) \\ &= \mathcal{F} \left[ \left( \mathcal{F}^{-1} \left[ q_k \hat{h}_k(t) \right] \right)^2 \right]. \end{aligned} \quad (16)$$

It is important to note that the Fourier modes  $\{\hat{h}_k(t)\}_{k=-N/2}^{N/2-1}$  are cyclic, and the quadratic term leads to a cyclic convolution

$$\hat{\mathcal{N}}_k(t) = - \left[ \sum_{k_1+k_2=k} + \sum_{k_1+k_2=k \pm N} \right] q_{k_1} q_{k_2} \hat{h}_{k_1}(t) \hat{h}_{k_2}(t). \quad (17)$$

The first sum in Eq. (17) is the right convolution sum whereas the second sum is called aliasing error. Specifically, the mode with wave number  $k_2 < -\frac{N}{2}$  is aliased to the mode with wave number  $k_2 + N$ , and the mode with wave number  $k_2 > \frac{N}{2} - 1$  is aliased to the mode with wave number  $k_2 - N$ . The method to eliminate the aliasing error is called de-aliasing. That is, we extend the vector  $\hat{h}_k(t)$  on both sides by zeros to make the  $N$  Fourier modes in the above centered convolution free of aliasing. The minimum and most efficient choice for  $M$  (expanded vector size) turns out to be  $3N/2$ , which is discussed in detail in Ref. [41].

### III. NUMERICAL RESULTS AND DISCUSSIONS

In our simulations, the time evolution of interface is started from an initially flat profile  $h(x, 0) = 0$  with periodic boundary conditions,  $\Delta x = 1$  and  $\Delta t = 0.05$ . Here, we only need to adjust the values of  $g$  for a given temporal correlated exponent. First, we ensure the simulated system into the true nonlinear KPZ scaling regime before numerical stability appearing. Then, we also need to make sure that the values of nonlinear strengths based on these two schemes are approximately equal for more reasonable comparison. It should be noted that there exists apparent singularity of growth, which indicates the genuine numerical instability intrinsic to the discretized nonlinear growth equations [36]. For simulating the temporal correlated KPZ equation, we find that numerical divergences are very evident using the standard FD scheme. Therefore, it is necessary to adopt appropriate numerical methods. We noticed that PS could control successfully numerical divergences in dealing with various local continuum growth systems, including KPZ with Gaussian white noise [39, 41, 43], adopting PS scheme becomes our first choice for simulating the temporal correlated KPZ equation, and fortunately, it could be effective to suppress numerical instabilities. For full comparison of the stability and reliability of numerical methods, LS scheme is also adopted to perform numerical investigations. Interestingly, our simulations show that LS scheme could also be effective in controlling numerical divergence even in the saturated growth regimes so that the scaling exponents could be obtained. In order to obtain the expected correlated noise from Eq. (7) with different temporal correlated exponent  $\theta$ , we set the value of  $N$  to 50 for high precision. We find that the spontaneous formation of faceted patterns becomes apparent in the long time limit as the correlated exponent  $\theta$  is increased. There will be evident change of the height profiles for  $\theta$  beyond a certain critical threshold  $\theta_{th}$ . Our results show that these interface profiles evolved from the temporal correlated KPZ system based on PS and LS schemes are consistent with each other, which are similar with the previous works with the same temporal correlated exponent and growth times[27, 30].

To quantitatively describe the scaling properties, we obtain growth exponent  $\beta$  with different  $\theta$  by computing the time evolution of interface width  $W(t)$  at the early growth time, and Fig. 1 depicts the results. We also find that, for the same  $\theta$ , different  $L$  yield similar  $\beta(L, t)$  curves, which means that finite-size effects are very weak.

In order to obtain  $\alpha$ , we need to calculate the saturated  $W(L, t)$  and then obtain scaling exponents based on Eq. (2) in different growth regimes. Considering large fluctuations of  $W(L, t)$  with system size and growth time, we adopt the large system sizes and noise realizations.

In our simulations, we calculate the scaling exponents  $\alpha, \beta, z$  with the discretized KPZ equation using both PS and LS schemes with  $\theta$  varying in the interval  $[0, 1/2]$ . In

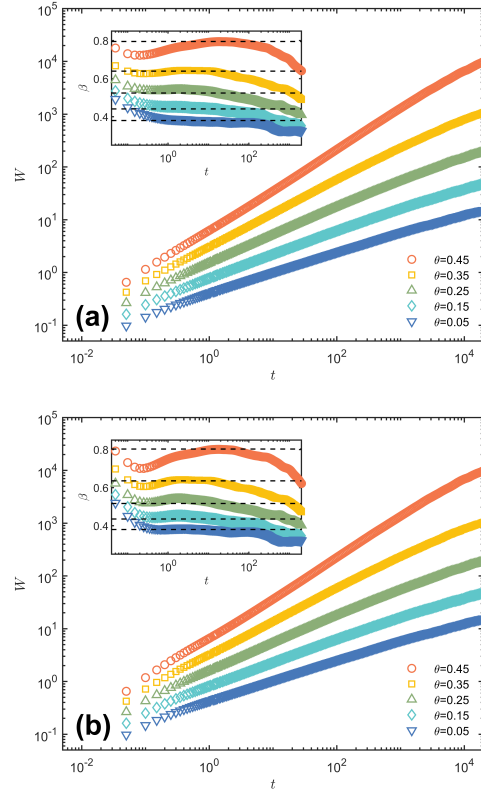


FIG. 1. The plot of interface width  $W(L, t)$  versus time  $t$  for the temporal correlated KPZ equation with (a) PS and (b) LS schemes. The insets show that we measure  $\beta$  during the plateau region. Here  $L = 16384$ , and the averages are taken over 250 realizations.

Fig. 2, we plot the independent results using these two schemes. Here  $\theta = 0.30$  is as a typical representative. In the early time regime  $t \ll L^z$ , we obtain the growth exponents  $\beta = 0.574 \pm 0.002$  for PS scheme, and  $\beta = 0.566 \pm 0.002$  for LS scheme. In the saturated growth regime  $t \gg L^z$ , we obtain the global roughness exponents  $\alpha = 0.773 \pm 0.006$  for PS scheme and  $\alpha = 0.770 \pm 0.005$  for LS scheme. Both PS and LS schemes obtain almost identical results.

Considering that the scaling exponents  $\alpha, \beta$ , and  $z$  are not independent, and there exists a simple way to collapse the data of Fig. 2 onto a single curve. In Fig. 3, we rescale the interface width  $W$  by  $W/L^\alpha$  vertically and rescale growth time  $t$  by  $t/L^z$  horizontally. A good collapse means that we choose effectively the values of  $\alpha$  and  $z$ .

In Fig. 4, our results show that the growth exponent varies distinctly with  $\theta$ . The scaling behavior has a very strong dependence on the long-range temporal correlations in the early growth regime. We find that the results calculated by PS scheme are very close to those by LS method, demonstrating that these two schemes are in well agreement with each other in simulating KPZ equation with long-range temporal correlations. When  $\theta$

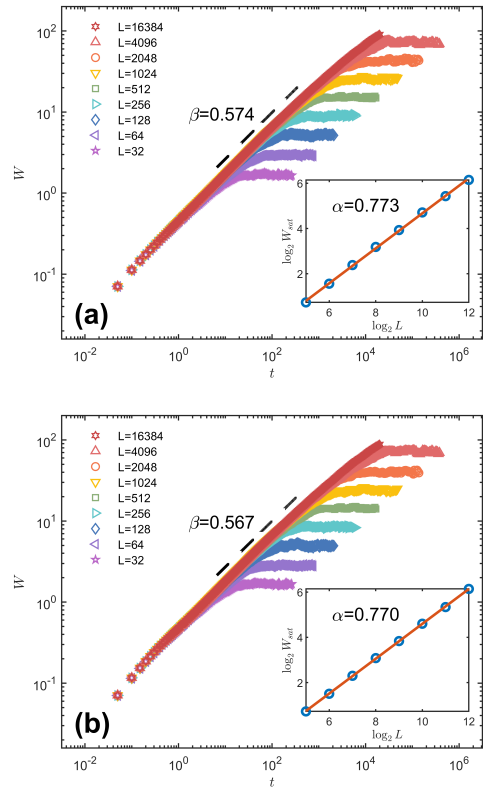


FIG. 2. The plot of  $W(L, t)$  at different growth regimes for  $\theta = 0.30$  using these two schemes: (a) PS and (b) LS. The dotted lines are the fitting results of  $\beta$ . The insets are the log-log plot of saturated interface width  $W_{sat}$  and system size  $L$ , and the solid lines are the fitting results of global roughness exponent  $\alpha$ . Data were averaged over 250 independent noise realizations. For the sake of clear comparison, each curve is shifted successively along the vertical coordinate.

approaches to 0, these results can be reduced to that of the normal KPZ equation using both PS and LS schemes. In the comparison with the previous theoretical predictions[6, 46, 50] and numerical simulations[28, 30], the growth exponents in this investigation are higher compared to those of other studies. And these results of dynamic exponents  $z$  match the SCE prediction. It should be noted that,  $\beta$  obtained here is larger than the results from simulating BD model in presence of temporally correlated noise. Thus, our results imply that, when the effects of long-range temporal correlation are not ignored, the continuum KPZ and discrete BD growth systems should not belong to the same universality class, even in presence of the same temporal correlated exponent. Interestingly, we noticed that previous works also show similar results. Peng et al.[13] suggested that BD driven by long-range spatially correlated noise does not belong to the spatial correlated KPZ universality class. The difference could be due to the different correlated noise generation methods, one needs to binarize the correlated noise into 0 or 1 in the modified BD system,

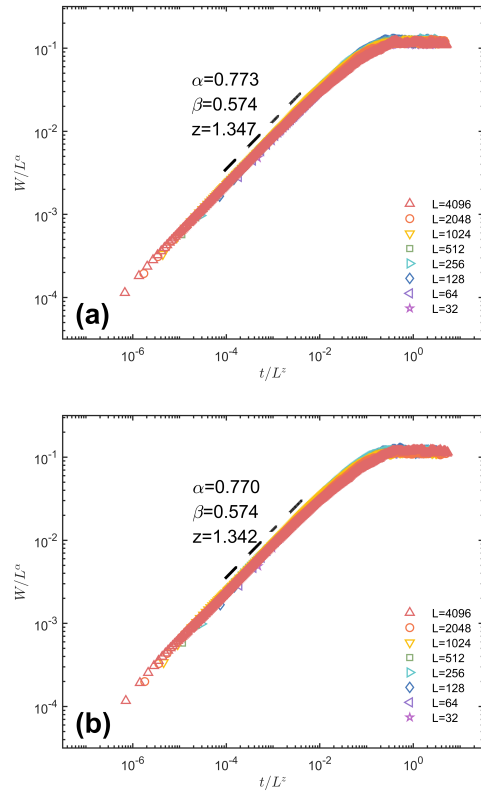


FIG. 3. The plot of the scaled interface width versus the scaled growth time. (a) and (b) are the results of data collapses corresponding to Figs. 2(a) and (b), respectively.

while we need not introduce this binarization in simulating temporal correlated KPZ equation based on the FFGN method.

Kinetically rough surfaces generated by Eq. (1) generally possess scale invariant properties. However, the existence of power-law scaling of the correlation functions does not determine a unique dynamic scaling form, which leads to the different anomalous forms of scaling[51]. One more independent exponent may be needed in order to assess the universality class of the particular system under study. Here, we recall some characteristic quantities in which the scaling behavior becomes manifest as a power law and define the relevant critical exponents. The equal-time height difference correlation function  $G(l, t)$  is the correlation between fluctuations of height between any two points  $x, x + l$ , which reads[52]

$$G(l, t) = \langle (h(x + l, t) - h(x, t))^2 \rangle. \quad (18)$$

The brackets  $\langle \dots \rangle$  denote average over noise. The local roughness exponent  $\alpha_{loc}$  is determined from the relation  $G(l, t) \sim l^{2\alpha_{loc}}$  ( $l \ll L$ ). A normal self-affine interface satisfies  $\alpha = \alpha_{loc}$ , and  $\alpha \neq \alpha_{loc}$  indicates anomalous scaling in surface growth. As shown in Fig. 5, we exhibit the plots of  $G(l, t)$  versus  $l$  with different growth times when  $\theta = 0.30$ . From the insets, it is obvious that the

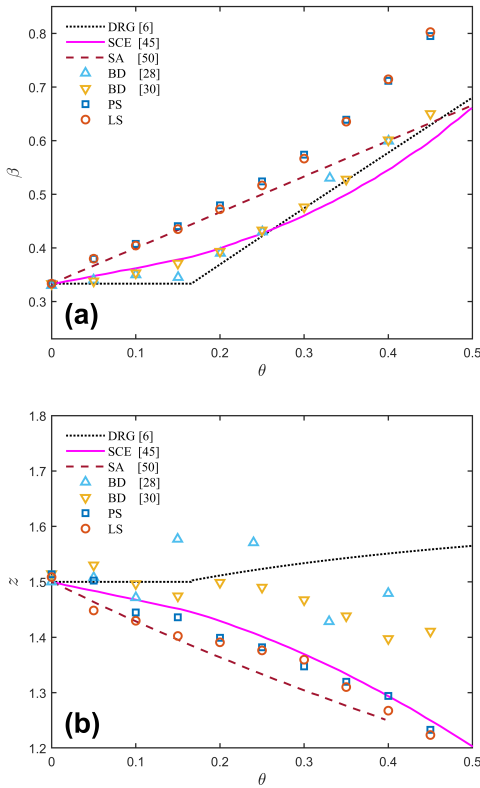


FIG. 4. (a) the growth exponent  $\beta$ , and (b) the dynamic exponent  $z$  as a function of the exponent  $\theta$  for decay of temporal correlations. Note that  $z$  was obtained from  $\alpha$  in Fig. 7 and  $\beta$  using the scaling relation  $z = \alpha/\beta$ .

slope curve has no plateau region when  $l \ll L$ , which means  $G(l, t)$  does not have an obvious power law relationship. This phenomenon occurs in the whole  $\theta$  region. Thus,  $\alpha_{loc}$  exhibiting non-universal scaling within local window sizes.

Apart from the height difference correlation function, one of the most general descriptions of the scaling properties in kinetic roughening is the structure factor, which reads[51]

$$S(k, t) = \langle \hat{h}_k(t) \hat{h}_{-k}(t) \rangle, \quad (19)$$

where  $\hat{h}_k(t)$  is the discrete Fourier coefficients obtained by Eq. (11). For  $(1+1)$ -dimensions, the structure factor satisfies the scaling form

$$S(k, t) = k^{-(2\alpha+1)} s(kt^{1/z}), \quad (20)$$

where the most general scaling function  $s(u)$ , consistent with scale-invariant dynamics, is given by[51]

$$s(u) \sim \begin{cases} u^{2(\alpha-\alpha_s)} & u \gg 1, \\ u^{2\alpha+1} & u \ll 1. \end{cases} \quad (21)$$

Here,  $\alpha_s$  is spectral roughness exponent. It is important to remark that  $S(k, t)$  allows one to obtain the distinc-

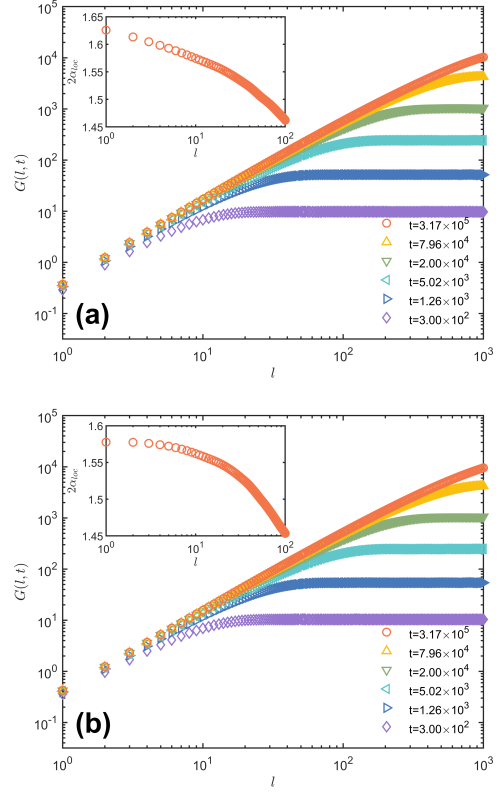


FIG. 5. The plot of height difference correlation function  $G(l, t)$  versus  $l$  for  $\theta = 0.30$  based on (a) PS and (b) LS schemes. The insets show that we measure  $\alpha_{loc}$  during the plateau region. Here  $L = 16384$ , and data were averaged over 250 independent noise realizations.

tively characteristic spectral roughness exponent  $\alpha_s$  typical of faceted growing surface, and  $\alpha_s$  leaves no trace in the usual height difference correlation functions[27]. Standard scaling corresponds to  $\alpha_{loc} = \alpha_s = \alpha < 1$ . However, other situations may be described within the generic scaling framework, including super-roughening ( $\alpha_{loc} = 1, \alpha_s = \alpha > 1$ ) and intrinsic anomalous scaling ( $\alpha_{loc} = \alpha_s < 1, \alpha_s \neq \alpha$ )[51]. To determine the universal critical properties, we utilize the power-law of the rescaled structure factor  $S(k, t)k^{2\alpha+1} \sim (kt^{1/z})^{2\alpha+1}$  for  $kt^{1/z} \ll 1$  and  $S(k, t)k^{2\alpha+1} \sim (kt^{1/z})^{2(\alpha-\alpha_s)}$  for  $kt^{1/z} \gg 1$ . When the roughness and dynamic exponents are chosen effectively, all the data collapses into a single universal curve for different wave number regimes. We can also check the dynamic exponent by  $z = \alpha/\beta$ .

Fig. 6 shows the plot of structure factor  $S(k, t)$ . We obtain  $\alpha_s = 0.831 \pm 0.003$  for PS scheme and  $\alpha_s = 0.827 \pm 0.003$  for LS method when  $\theta = 0.30$ . Based on data collapse, we find that the estimated values of  $\alpha_s$  here are larger than the actual calculated values of  $\alpha$  within the whole  $\theta$  region, and the evident difference between  $\alpha$  and  $\alpha_s$  implies anomalous scaling appearing in the KPZ system driven by long-range temporally correlated noise. For the global roughness exponents, we also find that  $\alpha$

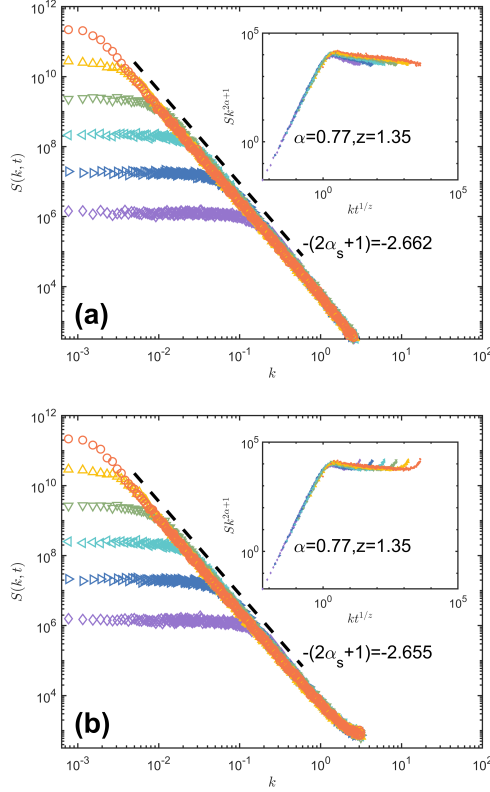


FIG. 6. The plot of structure factor  $S(k, t)$  versus  $k$  for  $\theta = 0.30$  using (a) PS and (b) LS schemes. Insets show the collapse of spectral densities using the critical exponents  $\alpha$  and  $z$ . Growth times and the independent noise realizations are the same as those in Fig. 5

versus  $\theta$  displays roughly the linearity relationship for the small  $\theta$  region, and our results agree with DRG for the large  $\theta$  region. Another interesting finding is that the slope of  $S(k, t)$  become smaller using PS scheme, but a little larger for adopting LS when  $kt^{1/z} \gg 1$ . Remarkably, the values of global roughness exponents are less than the corresponding spectral ones for the same  $\theta$ , as shown in Fig. 7. The difference between  $\alpha_s$  and  $\alpha$  becomes smaller as  $\theta \rightarrow 0$ , which means that the temporal correlated KPZ equation approaches to the normal KPZ equation.

#### IV. CONCLUSIONS

In this work, we performed numerically investigations of the KPZ equation with long-range temporally correlated noise in  $(1+1)$ -dimensions based on PS approach and LS discretization, one of the improved FD schemes. We show that the choice of numerical methods may be crucial in studying some physical properties of the non-linear stochastic growth systems. Long-range temporal correlations evidently affect the scaling properties of the KPZ system. Spontaneous formation of faceted

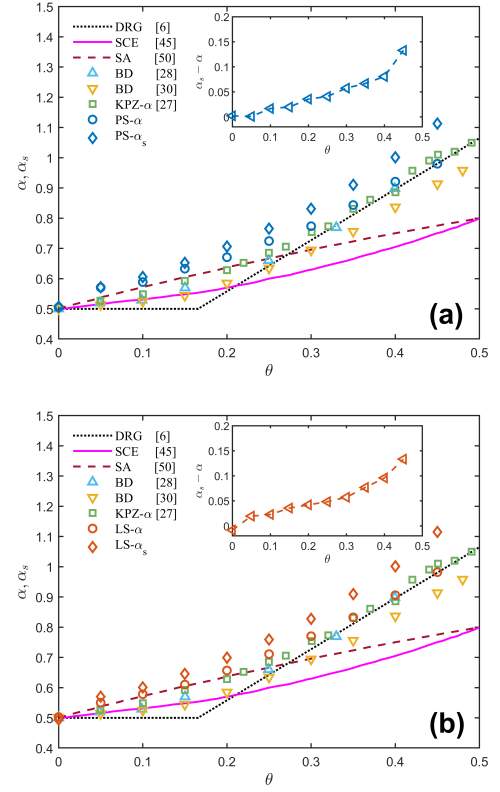


FIG. 7. The scaling exponents  $\alpha, \alpha_s$  versus  $\theta$  with (a) PS and (b) LS schemes. The existing predictions and numerical results of  $\alpha$  are also provided for comparison quantitatively. The insets show the difference of  $\alpha_s$  and  $\alpha$  versus  $\theta$  correspondingly.

patterns becomes apparent as the correlated exponent  $\theta$  is increased. As for scaling exponents  $\alpha, \beta$ , and  $z$ , we find that the results of PS and LS schemes are consistent with each other, demonstrating that these two schemes we adopted are reliable in simulating KPZ equation with long-range temporal correlations. When  $\theta$  approaches to 0, both PS and LS schemes can obtain the results of the normal KPZ equation with Gaussian white noise. Our results show that, the global roughness exponent  $\alpha$  versus  $\theta$  is linear fitted for the small  $\theta$  region, and agrees with DRG for the large  $\theta$  region, the growth exponent  $\beta$  in this investigations is higher compared to those of numerical studies based on BD in presence of long-range temporal correlations, and the results of dynamic exponent  $z$  match the SCE predictions, which is different from the previous results of direct simulating KPZ driven by temporally correlated noise adopted by exponential decaying technique to suppress numerical instability[27, 29]. Thus, our results show that, even in presence of the same temporally correlated noise, the scaling exponents from directly simulating KPZ are slightly different with those from the BD model. And our investigations also imply that, considering the possibility that relevant terms are spuriously introduced, for example, the exponentially

decaying function, the modified KPZ equation could not be considered as representative of the KPZ equation[38]. Further analysis show that there is no obvious power-law relationship in height difference correlation function  $G(l, t)$ , which implies  $\alpha_{loc}$  exhibiting non-universal scaling within local window sizes. By comparing these two characteristic roughness exponents  $\alpha_s$  and  $\alpha$ , we find that  $\alpha_s \approx \alpha$  in the very small  $\theta$  regions, and  $\alpha_s > \alpha$  in the large  $\theta$  regions. More precisely, the difference between  $\alpha_s$  and  $\alpha$  becomes larger as  $\theta$  increases.

It should be noted that numerical divergences always exists in simulating the temporal correlated KPZ equation using different numerical schemes, and the main cause of divergence is from the discretization of nonlinear term. Through full comparison, we find that adopting PS and LS schemes all could maintain evidently more long growth times than those using the standard FD methods. Fortunately, within the reasonable system sizes and growth times we chosen, the interface width could reach steadily the saturated regime using these two numerical schemes before numerical instability appearing, thus we could obtain successfully various scaling exponents. In-

terestingly, based on PS approach, this kind of numerical instability could be completely avoided in simulating the local growth equations, which was reported in the previous literatures[39–43]. Therefore, the range of validity and effectiveness of PS scheme remains elusive, and need to investigate utilizing various nonlinear stochastic systems, especially those including nonlocal interactions or long-range correlations. Furthermore, this work also motivates investigating alternative numerical methods for dealing with the nonlinear stochastic systems with long-range spatial or temporal correlations.

## ACKNOWLEDGMENTS

We would like to thank Juemin Yi and Yueheng Lan for useful discussions and critical reading of the manuscript. This work was supported by the Natural Science Foundation of Jiangsu Province under Grant No. BK20180637 and the National Natural Science Foundation of China under Grant No. 11804383.

---

[1] A.-L. Barabási and H. E. Stanley, *Fractal concepts in surface growth* (Cambridge university press, 1995).

[2] P. Meakin, P. Ramanlal, L. M. Sander, and R. Ball, *Physical Review A* **34**, 5091 (1986).

[3] M. Eden *et al.*, in *Proceedings of the fourth Berkeley symposium on mathematical statistics and probability*, Vol. 4 (1961) pp. 223–239.

[4] M. Kardar, G. Parisi, and Y.-C. Zhang, *Physical Review Letters* **56**, 889 (1986).

[5] F. Family and T. Vicsek, *Journal of Physics A: Mathematical and General* **18**, L75 (1985).

[6] E. Medina, T. Hwa, M. Kardar, and Y.-C. Zhang, *Physical Review A* **39**, 3053 (1989).

[7] P. Meakin and R. Jullien, *Europhysics Letters (EPL)* **9**, 71 (1989).

[8] T. Halpin-Healy, *Physical Review A* **42**, 711 (1990).

[9] P. Meakin and R. Jullien, *Physical Review A* **41**, 983 (1990).

[10] Y.-C. Zhang, *Physical Review B* **42**, 4897 (1990).

[11] J. G. Amar, P.-M. Lam, and F. Family, *Physical Review A* **43**, 4548 (1991).

[12] H. Hentschel and F. Family, *Physical Review letters* **66**, 1982 (1991).

[13] C.-K. Peng, S. Havlin, M. Schwartz, and H. E. Stanley, *Physical Review A* **44**, R2239 (1991).

[14] N.-N. Pang, Y.-K. Yu, and T. Halpin-Healy, *Physical Review E* **52**, 3224 (1995).

[15] M. S. Li, *Physical Review E* **55**, 1178 (1997).

[16] S. Mukherji and S. M. Bhattacharjee, *Physical Review letters* **79**, 2502 (1997).

[17] A. K. Chattopadhyay and J. Bhattacharjee, *Europhysics Letters (EPL)* **42**, 119 (1998).

[18] E. Frey, U. C. Täuber, and H. Janssen, *Europhysics Letters (EPL)* **47**, 14 (1999).

[19] H. Janssen, U. C. Täuber, and E. Frey, *The European Physical Journal B* **9**, 491 (1999).

[20] E. Katzav and M. Schwartz, *Physical Review E* **60**, 5677 (1999).

[21] M. K. Verma, *Physica A: Statistical Mechanics and its Applications* **277**, 359 (2000).

[22] E. Katzav, *Physical Review E* **68**, 046113 (2003).

[23] E. Katzav, *The European Physical Journal B* **54**, 137 (2006).

[24] E. Katzav, *Physica A: Statistical Mechanics and its Applications* **392**, 1750 (2013).

[25] T. Kloss, L. Canet, B. Delamotte, and N. Wschebor, *Physical Review E* **89**, 022108 (2014).

[26] S. Chu and M. Kardar, *Physical Review E* **94**, 010101 (2016).

[27] A. Alés and J. M. López, *Physical Review E* **99**, 062139 (2019).

[28] C.-H. Lam, L. M. Sander, and D. E. Wolf, *Physical Review A* **46**, R6128 (1992).

[29] T. Song and H. Xia, *Journal of Statistical Mechanics: Theory and Experiment* **2016**, 113206 (2016).

[30] T. Song and H. Xia, *Physical Review E* **103**, 012121 (2021).

[31] A. A. Fedorenko, *Physical Review B* **77**, 094203 (2008).

[32] P. Strack, *Physical Review E* **91**, 032131 (2015).

[33] D. Squizzato and L. Canet, *Physical Review E* **100**, 062143 (2019).

[34] M. Seeßelberg and F. Petruccione, *Computer Physics Communications* **74**, 303 (1993).

[35] K. Moser, J. Kertész, and D. E. Wolf, *Physica A: Statistical Mechanics and its Applications* **178**, 215 (1991).

[36] C. Dasgupta, J. M. Kim, M. Dutta, and S. Das Sarma, *Physical Review E* **55**, 2235 (1997).

[37] R. Gallego, M. Castro, and J. M. López, *The European Physical Journal B* **89**, 1 (2016).

- [38] B. Li, Z. Tan, Y. Jiao, and H. Xia, *Journal of Statistical Mechanics: Theory and Experiment* **2021**, 023210 (2021).
- [39] R. Gallego, M. Castro, and J. M. López, *Physical Review E* **76**, 051121 (2007).
- [40] A. Giacometti and M. Rossi, *Physical Review E* **63**, 046102 (2001).
- [41] L. Giada, A. Giacometti, and M. Rossi, *Physical Review E* **65**, 036134 (2002).
- [42] Priyanka, U. C. Täuber, and M. Pleimling, *Physical Review E* **101**, 022101 (2020).
- [43] R. Gallego, *Applied Mathematics and Computation* **218**, 3905 (2011).
- [44] D. Roy and R. Pandit, *Physical Review E* **101**, 030103 (2020).
- [45] C.-H. Lam and F. G. Shin, *Physical Review E* **57**, 6506 (1998).
- [46] E. Katzav and M. Schwartz, *Physical Review E* **70**, 011601 (2004).
- [47] B. B. Mandelbrot, *Water Resources Research* **7**, 543 (1971).
- [48] B. B. Mandelbrot and J. R. Wallis, *Water Resources Research* **5**, 228 (1969).
- [49] H. A. Makse, S. Havlin, M. Schwartz, and H. E. Stanley, *Physical Review E* **53**, 5445 (1996).
- [50] Hanfei and B. Ma, *Physical Review E* **47**, 3738 (1993).
- [51] J. J. Ramasco, J. M. López, and M. A. Rodríguez, *Physical Review letters* **84**, 2199 (2000).
- [52] J. M. López, M. A. Rodríguez, and R. Cuerno, *Physical Review E* **56**, 3993 (1997).